PERGAMON

International Journal of Solids and Structures 38 (2001) 5303–5322

INTERNATIONAL JOURNAL OF SOLIDS and STRUCTURES

www.elsevier.com/locate/ijsolstr

Fracture parameters of interfacial crack of bimaterial under the impact loading

Dong Kil Shin, Jung Ju Lee *

Department of Mechanical Engineering, Korea Advanced Institute of Science and Technology, 373-1 Kusong-dong, Yusong-gu, Taejon 305-701, South Korea

Received 28 December 1999

Abstract

The impact responses of the fracture parameters of interfacial crack tip, such as energy release rate (J integral), stress intensity factors (K), crack opening displacement (COD) and T stress, under the dynamic loading condition were studied using both numerical and experimental methods. A three point bending impact test was performed with bimaterial specimens composed of aluminum and polymethyl methacrylate (PMMA). Fracture parameters for the interfacial crack tip were calculated by a programmed post processor which used both the domain integral method and the interaction energy method. The interaction energy method showed good performance in the decomposition of stress intensity factor and the calculation of elastodynamic T stress with path independency. The phase angle of stress intensity factor varied with time. The relationship between energy release rate and phase angle at the onset of crack propagation showed unsymmetrical U shaped curve. COD showed same result with the result of stress intensity factors. The magnitude of the T stress was not enough to affect the plastic deformation. Specimens whose T stress were less than zero exhibited stable crack growth along the interface as expected in the analysis. © 2001 Published by Elsevier Science Ltd.

Keywords: Dynamic fracture; Low velocity impact; Interaction energy method; Energy release rate; Stress intensity factor; Crack opening displacement; T stress

1. Introduction

Studies on the failures by impact loading have been reported more frequently as the speed of mechanical systems become faster. If the loading time in reaching a maximum is shorter than the natural frequency of the body, then the effect of material inertia becomes very important, therefore wave propagation must be considered in the analysis. Stress fields of dynamic loading which differ from the static condition are formed by elastic waves which are scattered at the crack tip and also bounded at the boundary. To analyze this dynamic crack problem, dynamic fracture mechanics have been applied to various research topics such as wave propagation, crack initiation, propagation, arresting, kinking, curving, branching and so on (Freund, 1990).

* Corresponding author. Tel.: +82-42-869-3033; fax: +82-42-869-3210/5210.
E-mail address: jjlee@sorak.kaist.ac.kr (J.J. Lee).

0020-7683/01/$ - see front matter © 2001 Published by Elsevier Science Ltd.
PII: S0020-7683(00)00399-1

Energy release rate (J integral), stress intensity factors (K), and crack opening displacement (COD) are important fracture parameters not only in the static fracture but also in the dynamic fracture. Kishimoto et al. (1980) expanded the static J integral to the dynamic problem. Li et al. (1985) showed that the line integral form of a J integral could be changed to the area integral in the plane problem using the weight function q. T stress, the second term of Williams' series expansion, has received attention as the second fracture parameter, because the shape and the size of plastic deformation area can be changed by the magnitude of T stress and crack stability is influenced by the sign of T stress (Larsson and Carlsson, 1973). Many researchers have tried to obtain the T stress more simply and exactly. Cardew et al. (1985) showed that the interaction integral method could be used to calculate T stress.

Recently, a reliability assessment of bimaterial under the impact loading has become very important, because bimaterials are widely used in various engineering structures, such as military armor, transportation vehicles, aerospace, electronic packages and so on. Researches about the fracture parameters of bimaterial have been performed in various ways, since the experimental study of Tippur and Rosakis (1991). They measured stress field and energy release rate from the bimaterial including the interfacial crack. Thereafter, Lo et al. (1994) calculated the energy release rate and stress intensity factors using both a domain integral method and an interaction energy method. Recently, Tippur and Xu (1997) performed a three point bending impact test and showed that the energy release rate at the crack initiation time (J_{ID}) was associated with phase angle, as the static result of Liechti and Chai (1992) also showed. Kavaturu and Shukla (1998) reviewed COD in the dynamic interfacial crack propagation and proposed that vectorial COD before and after crack initiation was a useful fracture parameter. Sladek et al. (1997) analyzed T stress by interaction integral method about the homogeneous material under the dynamic condition.

Although, several reports associated with both theoretical and numerical studies on the impact fracture of bimaterial have been reported, few dynamic experimental results with numerical analysis are found as compared with the static results. Therefore, we studied the fracture parameters of crack tip, such as energy release rate, stress intensity factors, COD and T stress, under the condition of a dynamic fracture, using numerical and experimental method. We confined this study to low velocity impact and fracture parameters at the onset of cracking. Firstly, we performed experiments using bimaterial specimens under a mixed mode impact loading. Secondly, we analyzed the dynamic problem using FEM. Finally, we calculated the elastodynamic J integral, stress intensity factors, COD and T stress using both a domain integral method and an interaction energy method with a programmed post processor. The post processor performed calculations using data such as coordinates, displacements, velocities, accelerations, and stresses obtained from the commercial FEM package program (ABAQUS). In the interaction energy method, auxiliary fields, formed by the point force at the crack tip, were also used to calculate T stress. Auxiliary fields, formed by the far field pure mode I and mode II, were used to calculate the stress intensity factors.

2. Review of fracture parameters in dynamic fracture mechanics

2.1. Stress fields around the interfacial crack tip

According to the results of the solution of Williams (1957), the stress field around the crack tip of a plate under symmetric loading is written as follows

$$\sigma_{ij} = A_{ij}(\theta) r^{-(1/2)} + B_{ij}(\theta) + C_{ij}(\theta) r^{1/2} + \cdots \tag{1}$$

where r, θ and σ_{ij} are cylindrical coordinates and the stress tensor respectively. A_{ij}, B_{ij}, and C_{ij} are universal functions of θ. The first term includes the stress intensity factor K and $-1/2$ singularity order, and the second term is so called T stress (Rice, 1974).

Linear elastic fracture mechanics (LEFM) is based on the assumption that the stress field near the crack tip could be characterized by a single parameter, stress intensity factor K. Therefore under a small scale yielding condition, the first term of a Williams' series was sufficient to describe the crack tip. However, Larsson and Carlsson (1973) showed that the first term was not sufficient to describe the stress field of various types of finite specimens, and the area of plastic deformation could be changed by the sign and magnitude of T stress. They also showed that the second term should be added to the boundary tractions for the boundary layer problem. Following their study, Rice (1974) showed the effects of T stress for a simple biaxial tension model.

In the case of dynamic condition, stress fields around the interfacial crack tip of bimaterial including T stress before the crack initiation (stationary crack), could be written as follows (Moon and Earmme, 1998)

$$\sigma_{ij}(r,\theta,t;\varepsilon) = \frac{\mathrm{Re}[K(t)r^{i\varepsilon}]}{\sqrt{2\pi r}}\tilde{\sigma}_{ij}^{\mathrm{I}}(\theta;\varepsilon) + \frac{\mathrm{Im}[K(t)r^{i\varepsilon}]}{\sqrt{2\pi r}}\tilde{\sigma}_{ij}^{\mathrm{II}}(\theta;\varepsilon) + T_m(t)\delta_{1i}\delta_{1j} \tag{2}$$

where, $K = K_1 + \mathrm{i}K_2$, δ, $m(=1,2)$ and t are the complex stress intensity factor, Kronecker delta, each material and time, respectively. $\tilde{\sigma}_{ij}$ is universal function of θ (Suo, 1989). This equation is similar with the case of the static condition except that K and T are time dependent. Oscillation index ε and Dunders' parameter β are

$$\begin{aligned}
\varepsilon &= \frac{1}{2\pi}\ln\frac{1+\beta}{1-\beta} \\
\alpha &= \frac{\mu_2(\kappa_1+1)-\mu_1(\kappa_2+1)}{\mu_2(\kappa_1+1)+\mu_1(\kappa_2+1)} \\
\beta &= \frac{\mu_2(\kappa_1-1)-\mu_1(\kappa_2-1)}{\mu_2(\kappa_1+1)+\mu_1(\kappa_2+1)} \\
\kappa_j &= \begin{cases} 3-4\nu_j & \text{plane strain} \\ \frac{3-\nu_j}{1+\nu_j} & \text{plane stress} \end{cases}
\end{aligned} \tag{3}$$

where μ and ν are shear modulus and Poisson's ratio, respectively.

2.2. Fracture parameters of dynamic fracture mechanics

Energy release rate is an important fracture parameter of dynamic problem as well as static. According to Atluri (1986), the energy release rate under the dynamic loading condition can be written as

$$G \equiv \lim_{\varepsilon\to 0}\int_{\Gamma_\varepsilon}\left[(W+T)n_1 - t_i\frac{\partial u_i}{\partial x_1}\right]\mathrm{d}s \tag{4}$$

where

$$W = \int_{-\infty}^{t}\sigma_{ij}\frac{\partial^2 u_i}{\partial t'\partial x_j}\mathrm{d}t', \qquad T = \frac{1}{2}\rho\frac{\partial u_i}{\partial t}\frac{\partial u_i}{\partial t} \tag{5}$$

and Γ_ε, ε, n, t, u, ρ are integration path, radius of path, normal vector, traction, displacement and material density, respectively.

Eq. (4) is an improper expression for the numerical approach, therefore Li et al. (1985) and Shih et al. (1986) changed this equation to a domain integral using a weight function q_i, based on the virtual crack extension method. As a result, energy release rate can be written as

$$G = \lim_{\varepsilon\to 0}\int_{\Gamma_\varepsilon}\left[\sigma_{ij}n_j\frac{\partial u_i}{\partial x_1} - (W+T)n_1\right]q_1\,\mathrm{d}s$$
$$= \int_A\left[\sigma_{ij}\frac{\partial u_i}{\partial x_1}\frac{\partial q_1}{\partial x_j} - (W+T)\frac{\partial q_1}{\partial x_1} + \rho\left(\frac{\partial^2 u_i}{\partial t^2}\frac{\partial u_i}{\partial x_1} - \frac{\partial u_i}{\partial t}\frac{\partial^2 u_i}{\partial x_1\partial t}\right)q_1\right]\mathrm{d}A \tag{6}$$

Lo et al. (1994) showed that J based interaction energy of the current field, A, and auxiliary field, B, could be written as

$$J^{\mathrm{I}} = \lim_{\varepsilon\to 0}\int_{\Gamma_\varepsilon}\left\{\sigma_{ij}^A\varepsilon_{ij}^B n_1 - \left(\sigma_{ij}^A u_{i,1}^B + \sigma_{ij}^B u_{i,1}^A\right)n_j + \rho\frac{\partial u_i^A}{\partial t}\frac{\partial u_i^B}{\partial t}n_1\right\}\mathrm{d}\Gamma \tag{7}$$

Similarly to Eq. (6), this Eq. (7) can be rewritten as

$$J^{\mathrm{I}} = \int_A\left[\begin{array}{l}\left(\sigma_{ij}^A\frac{\partial u_i^B}{\partial x_1} + \sigma_{ij}^B\frac{\partial u_i^A}{\partial x_1}\right)\frac{\partial q}{\partial x_j} - \left(\sigma_{ij}^A\varepsilon_{ij}^B + \rho\frac{\partial u_i^A}{\partial t}\frac{\partial u_i^B}{\partial t}\right)\frac{\partial q}{\partial x_1}\\ +\rho\left(\frac{\partial^2 u_i^A}{\partial t^2}\frac{\partial u_i^B}{\partial x_1} + \frac{\partial^2 u_i^B}{\partial t^2}\frac{\partial u_i^A}{\partial x_1} - \frac{\partial^2 u_i^A}{\partial x_1\partial t}\frac{\partial u_i^B}{\partial t} - \frac{\partial u_i^A}{\partial t}\frac{\partial^2 u_i^B}{\partial x_1\partial t}\right)q\end{array}\right]\mathrm{d}A \tag{8}$$

When we choose bimaterial stress field (Suo, 1989) as an auxiliary field, and consider pure mode I ($B_1, K = 1 + \mathrm{i}0$) and mode II ($B_2, K = 0 + \mathrm{i}1$), stress intensity factors and global phase angle can be written as

$$K_1^A = \frac{8\cosh^2(\pi\varepsilon)}{c_1+c_2}J^{A,B_1}, \qquad K_2^A = \frac{8\cosh^2(\pi\varepsilon)}{c_1+c_2}J^{A,B_2}$$
$$\phi = \tan^{-1}\left(\frac{K_2}{K_1}\right) \tag{9}$$

where J^{A,B_1} and J^{A,B_2} are interaction energies of AB_1 and AB_2 and

$$c_i = \frac{1+\kappa_i}{\mu_i} \tag{10}$$

Rice (1988) proposed a complex stress intensity factor which had same physical dimension with the stress intensity factor of homogeneous material.

$$Kr^{i\varepsilon} = K_{\mathrm{I}} + \mathrm{i}K_{\mathrm{II}} \tag{11}$$

Local phase angle of stress intensity factor at characteristic length $\hat{r}$ is defined as

$$\psi|_{r=\hat{r}} = \tan^{-1}\left(\frac{\mathrm{Im}[K\hat{r}^{i\varepsilon}]}{\mathrm{Re}[K\hat{r}^{i\varepsilon}]}\right) = \phi + \varepsilon\ln(\hat{r}) \tag{12}$$

As shown in Eq. (12), phase angle is dependent on characteristic length $\hat{r}$.

COD at the interfacial crack is written as (Rice, 1988)

$$\delta_1 + \mathrm{i}\delta_2|_{r=\hat{r}} = \frac{(c_1+c_2)\sqrt{\hat{r}}}{2\sqrt{2\pi}}\left[\frac{K\hat{r}^{i\varepsilon}}{1+2i\varepsilon}\right] \tag{13}$$

When we adopt the stress field of bimaterial interfacial crack under the point force, f, as an auxiliary field, T stress could be written as follows (Moon and Earmme, 1998)

$$T_i = \frac{1}{f}E_i' J^{\mathrm{I}} \tag{14}$$

where

$$E_i' = \begin{cases} E_i/(1-v_i^2) & \text{plane strain} \\ E_i & \text{plane stress} \end{cases} \tag{15}$$

and E is elastic modulus.

Each T stress has the following relationship

$$T_2 = \frac{1-\alpha}{1+\alpha} T_1 \tag{16}$$

where α is Dunders' parameter in Eq. (3). Material properties E and v are known and the point force, f, can be set to unity. Leevers and Radon (1982) defined biaxility parameter, B, by normalizing the T stress with stress intensity factor, K,

$$B = \frac{T\sqrt{\pi a}}{K} = \frac{T\sqrt{\pi a}}{\sqrt{J\frac{16\cosh^2(\pi\varepsilon)}{c_1+c_2}}} \tag{17}$$

3. Experiment

An impact test was performed with a Dynatup 8250 (Instron Co.). The mass of the impactor was 5.41 kg and the impact velocity was 2.17 m/s. The impact load was measured at the mid-position of tup by the load cell at every 0.5 μs. Impact velocity was measured by the photo detector just before the tup impacts the specimen. Crack initiation time was measured by a conductive grid technique (Dotite, electro-conductive) to exclude the reinforcement effect of strain gauge, and signals were stored in the personal computer via a digital oscilloscope with 5 M sample per s sampling rate. Fig. 1 shows a schematic diagram of the experimental setup.

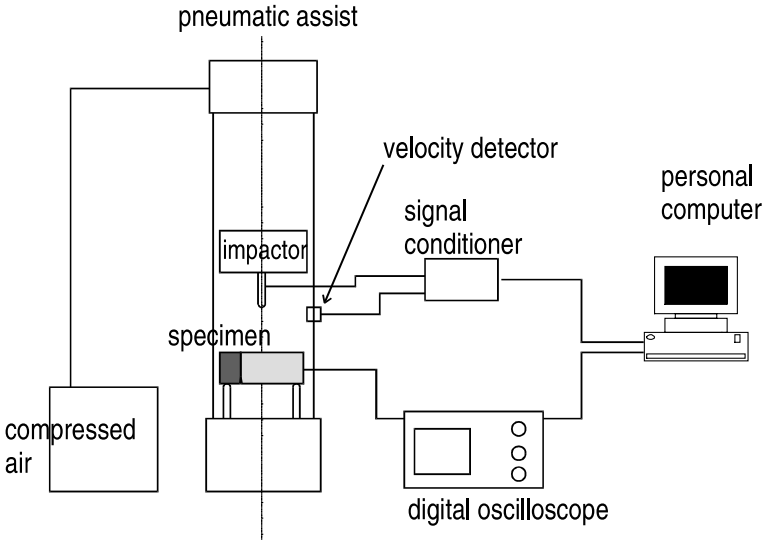

Fig. 1. Schematic diagram of experimental setup.

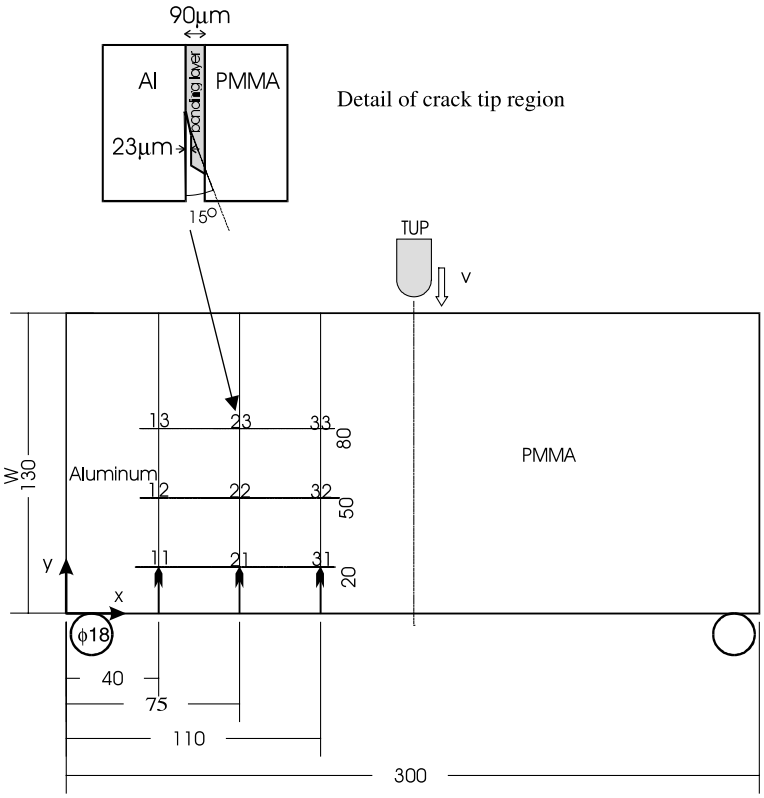

Fig. 2. Dimensions of specimen and the sharpness of crack tip.

Aluminum 6061-T6 and (polymethyl methacrylate (PMMA), Hanhwa Co.) that had a 130 mm height and 7.8 mm thickness were cut by a diamond cutting machine according to the designed size. The widths of aluminum were 40, 75, and 110 mm, and the widths of PMMA were 260, 225, and 190 mm. Then two materials were bonded as shown in Fig. 2 resulting in a 300 mm width. The contact surface of aluminum was treated by a sand blaster and the PMMA was treated by an abrasive sand paper #220. The initial crack was made by using Teflon film (23 μm thickness) which was inserted into the interface before the bonding process and removed before the test. Teflon film was cut by sharp razor and then the sharpness of Teflon insert was checked in detail. Cut face had about 15° of sharpness, which was same order of sharpness of razor blade as shown in Fig. 2. Initial crack lengths were 20 ($a/W = 0.154$), 50 ($a/W = 0.383$), and 80 mm ($a/W = 0.615$). Aluminum and PMMA were bonded by a commercial acrylic adhesive 'Weld-On 10' (IPS Corp.), which was composed of a PMMA monomer and catalyst. Adhesive was polymerized at room temperature over 48 h. The thickness of the bonding layer was about 90 μm.

4. FEM analysis

The dynamic response of the interfacial crack tip of bimaterial was analyzed by use of commercial FEM package program ABAQUS/implicit. Fracture parameters were calculated by the programmed post processors, which used data such as coordinates, displacements, velocities, accelerations, and stresses obtained from the ABAQUS. Material properties are shown in Table 1. Fig. 3 shows the FEM model, crack tip

Table 1
Material properties of bimaterial (PMMA and aluminum)

Property	PMMA	Aluminum
E (GPa)	3.02	80.0
v	0.35	0.33
c_l (m/s) (plane stress)	1700	5755
c_s (m/s)	970	3331
c_R (m/s)	906	3105
ρ (kg/m^3)	1190	2710

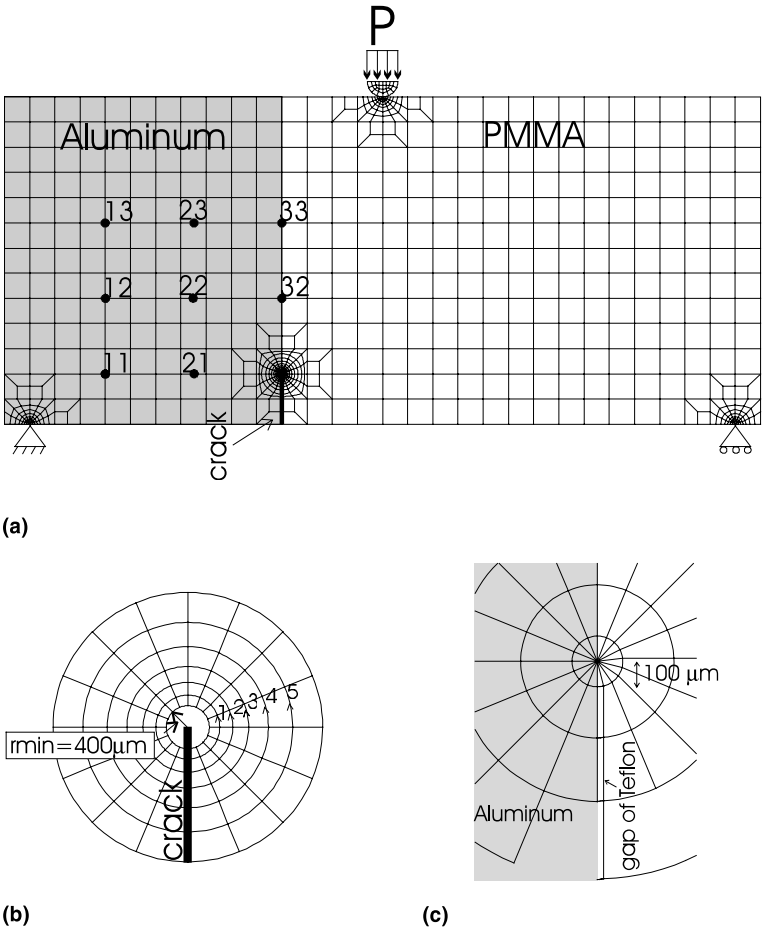

Fig. 3. FEM model, crack tip positions, and integration paths of bimaterial specimen (a) FEM model of TIP_{31}; (b) Crack tip of crack model; (c) Crack tip of wedge model.

positions, and the integration paths of the bimaterial specimen. Crack tip positions are marked as TIP_{ij} where i is the index of x position, and j is the index of y position. Eight node quadratic plane stress elements were used for this model, except for the crack tip region where degenerated quadratic elements were used. Singular element at the crack tip was not used. Interpenetrating of crack faces was allowed because crack

face of PMMA was deformed by the crack closing force during the some time of interval. Actually, contact was not occurred because the initial clearance existed about 23 μm of Teflon film thickness and 90 μm of total bonding thickness as shown in Fig. 2. Two types of crack tip were modeled. One was crack model, which was used to calculate fracture parameters. The other was wedge model, which modeled real crack tip and was used to check the contact of crack faces and suitability of FEM model. However, fracture parameters (J, K, T) were nearly same for each other because existing clearance was too small compared with the dimension of specimen. In the crack model, the nearest elements to the crack tip ($r = 400$ μm) were excluded in the calculation. In the wedge model, the tip of cut Teflon film was modeled. Film thickness was 23 μm and wedge length was 100 μm. We assumed that two points at the base of the specimen were simply supported because the specimen was supported by two rollers. Load history, which was measured in the test, was applied to the tup by the pressure load in the FEM analysis. Contact conditions between tup and specimen were as follows. Finite sliding was allowed, slip tolerance was 0.8, and the friction coefficient was 0.3. In this analysis, we assumed that the Hilber–Hughes parameter was -0.02 and maximum time step was 2 μs. Under the assumption that crack initiates when J reached critical value, crack initiation toughness J_{ID}, we determined the calculated J value at the measured crack initiation time to be J_{ID}.

5. Experimental and numerical results

Fig. 4 shows the load history measured at the middle of the impact tup. It is generally reported that the load history at the impact position shows the behavior of $\sin^a(t)$ curve, according to the Hertzian contact theory (Johnson, 1987). However, in this experiment, the measurement of load at the impact position was very hard, because the load cell was located at a distance of about 13 cm from the impact position. Therefore the arrival time of dilatational wave was delayed about 18 μs. The increasing patterns of load are similar for all types of specimen. Load signals reach peaks about 0.2 ms, with the same inclination and roughly the same magnitude. And then load diminishes to zero after showing one or two more peaks. However, in the case of TIP_{11}, the load increases to 8 kN again. This behavior of TIP_{11} means that the specimen was fractured after several rebounds of the elastic wave, because the crack tip position of TIP_{11} was the farthest from the impact point in nine crack tip positions.

Three fractured specimens TIPs 11, 12 and 13 are filed up to compare the crack path as shown in Fig. 5. Typical examples of crack propagation paths are shown in Fig. 6. Crack initiates at critical J_{ID} and then propagates along the interface for some distance. After that, crack kinks to the PMMA and then propa-

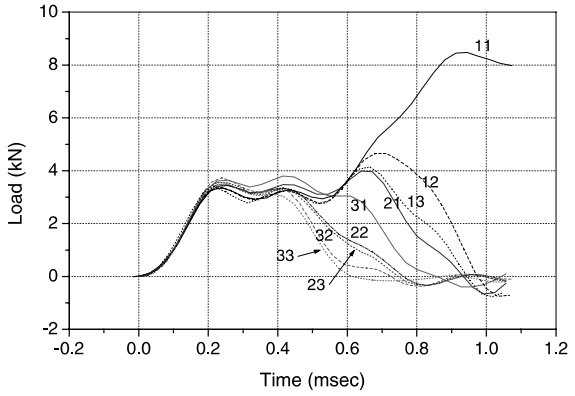

Fig. 4. Measured impact load variation over time.

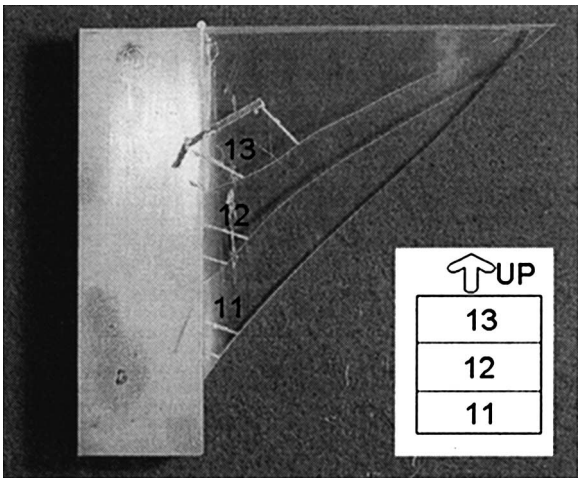

Fig. 5. Fractured specimen of TIPs 11, 12, and 13.

gates toward the impact position. The length that the crack propagates along the interface was varied with types of specimens. For example, at the specimen of TIP_{13}, the crack almost directly kinked to PMMA part as shown in Fig. 6(a). However, at the specimen TIP_{31}, the crack propagated along the interface over 10 mm as shown in Fig. 6(b). At the crack tip position TIP_{11}, only one of five specimens was fractured at the impact energy level (12.7 J, $v = 2.17$ m/s). When we increased the impact velocity to $v = 5$ m/s, the initial fracture did not occur at the interface crack but occurred at the impact position with circular shape and the crack started to propagate downward as shown in Fig. 6(c). In addition, local plastic deformation was observed at the impact position of PMMA at both static and dynamic experiments of TIP_{11}. Therefore it is hard to regard TIP_{11} as a low velocity elastic impact.

Fig. 7 shows the variation curves of the energy release rate (J) over time at the interface crack tip of the bimaterial specimens under the impact load. In these figures, a solid line shows the J curve before the crack initiation. Cross symbol ($\times$) represents the onset of crack initiation. Dotted line after the symbol ($\times$) shows J value of the case if the crack does not initiate. The load reaches a peak in about 0.2 ms as shown in Fig. 4. However the effect of J is not shown until this time (0.2 ms). The dilatational wave can travel through the height of PMMA 3.1 times during this 0.2 ms. The time, when the effect of J is observed, becomes faster as the distance from the impact position to the crack tip becomes shorter. At first, we expected that the crack initiation time of TIP_{i3} (13, 23, and 33) might be faster than TIP_{i2} (12, 22, and 32) respectively, because the distances of TIP_{i3} from crack tip to impact position were shorter than those for TIP_{i2}. However, the crack initiation times of TIP_{i2} were faster than TIP_{i3} in this experiment. This situation will be explained later alone with the results of phase angle effect. According to the results of the J variation of TIP_{11} in Fig. 7(a), it can be said that specimen of TIP_{11} was fractured after several fluctuations of J.

Fig. 8 shows the variation curves of stress intensity factors and phase angle, ψ, where $K_{\mathrm{I}} = \mathrm{Re}[K\hat{r}^{i\varepsilon}]$, $K_{\mathrm{II}} = \mathrm{Im}[K\hat{r}^{i\varepsilon}]$ and $\hat{r}$ (=1000 μm) is characteristic length. As shown in Eq. (11), stress intensity factor and phase angle are dependent on the characteristic length. Two types of characteristic length can be chosen. One is specimen based length scale such as crack length, specimen thickness, and so on. The other is material based length such as 1, 100 μm, grain size, and so on. In this study, crack tip positions and crack lengths are different, and fracture parameters on crack initiation time are important. Plastic zone size in TIP_{22} at crack initiation time was about 500 μm. Therefore we chose 1000 μm which was twice of the plastic zone size. Tippur and Xu (1997) had selected 1000 μm and Lambros and Rosakis (1995) had selected 2000 μm for similar experimental condition. Shear term K_{II} increases with time increases by the external load and

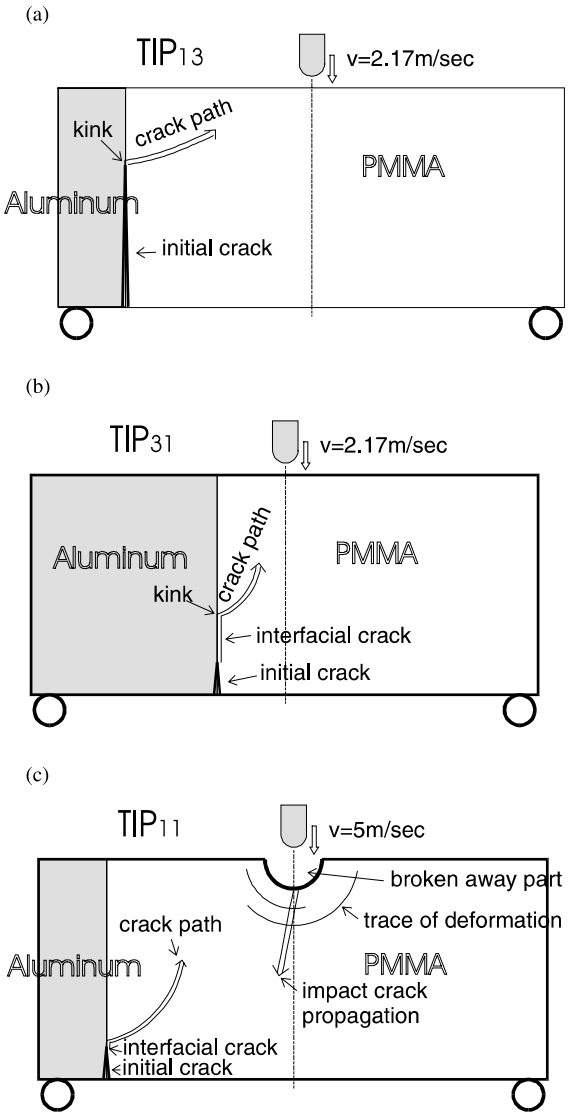

Fig. 6. Schematic diagram showing crack propagation path of bimaterial specimen (a) TIP_{13}, (b) TIP_{31}, (c) TIP_{11}.

decreases by decreasing external load. However, K_I has minus value initially during about 0.2–0.4 ms and then increases until fracture occurs. This means that, compression mode ($K_I < 0$) is formed by elastic wave. Under the static condition, only opening mode is occurred in this case of bending specimen. However, closing mode as well as opening mode can be occurred under the dynamic condition by the time when stress waves arrive. Mode mixity has minus value by Eq. (12) when K_I has minus value and K_{II} has plus value, but it only means shifting of phase angle. Therefore, we added 180° in this case to have continuity. Phase angle has large value initially, and decreases with time. This result agrees with the numerical result of Lo et al. (1994). Note that Lo et al. used initial crack length as characteristic length.

The effect of crack closure by minus K_I is observed more clearly in the specimen which has long initial crack length. Fig. 9 shows the deformed shape of specimen (magnification factor: ×200) when K_I has

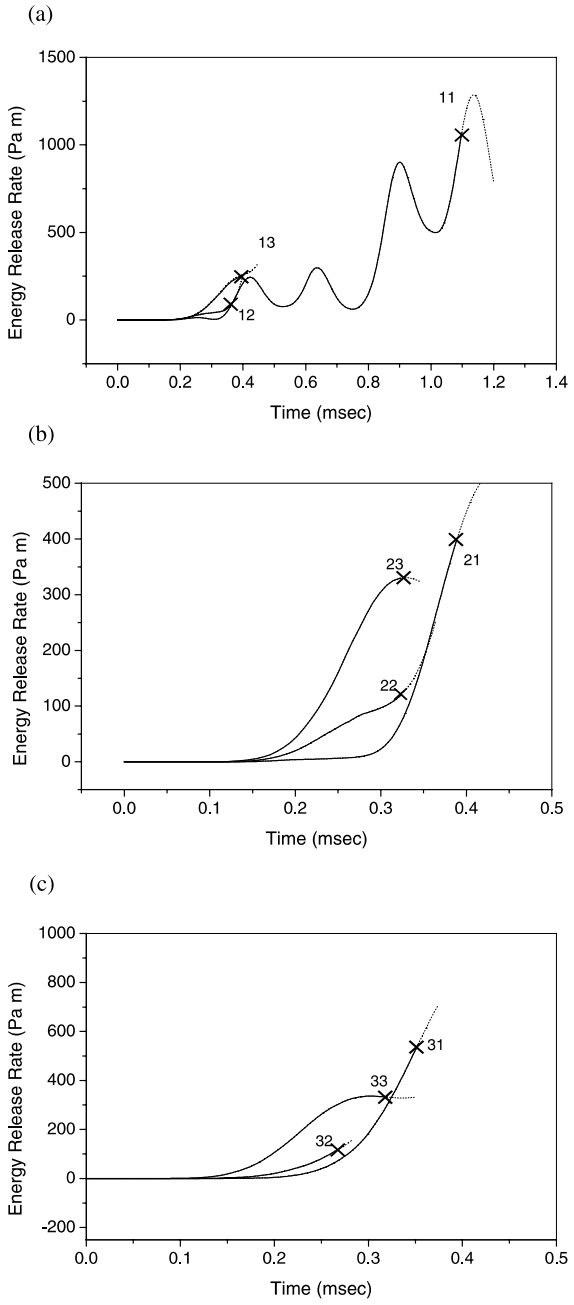

Fig. 7. Energy release rate variation curve over time. (a) TIP_{1j}, (b) TIP_{2j}, (c) TIP_{3j} ($\times$ represents the onset of crack initiation).

minimum value for (a) TIP_{23} (0.280, 0.320 ms) and (b) TIP_{21} (0.22, 0.39 ms). Compliant part of interfacial crack (PMMA) is deformed to down by shear effect, and deformed to left by compression effect. Initial clearance about 23 μm thickness and 10 mm length was located below the crack tip by removed Teflon film, and initial clearance about 90 μm thickness was located below the remained crack region. Therefore,

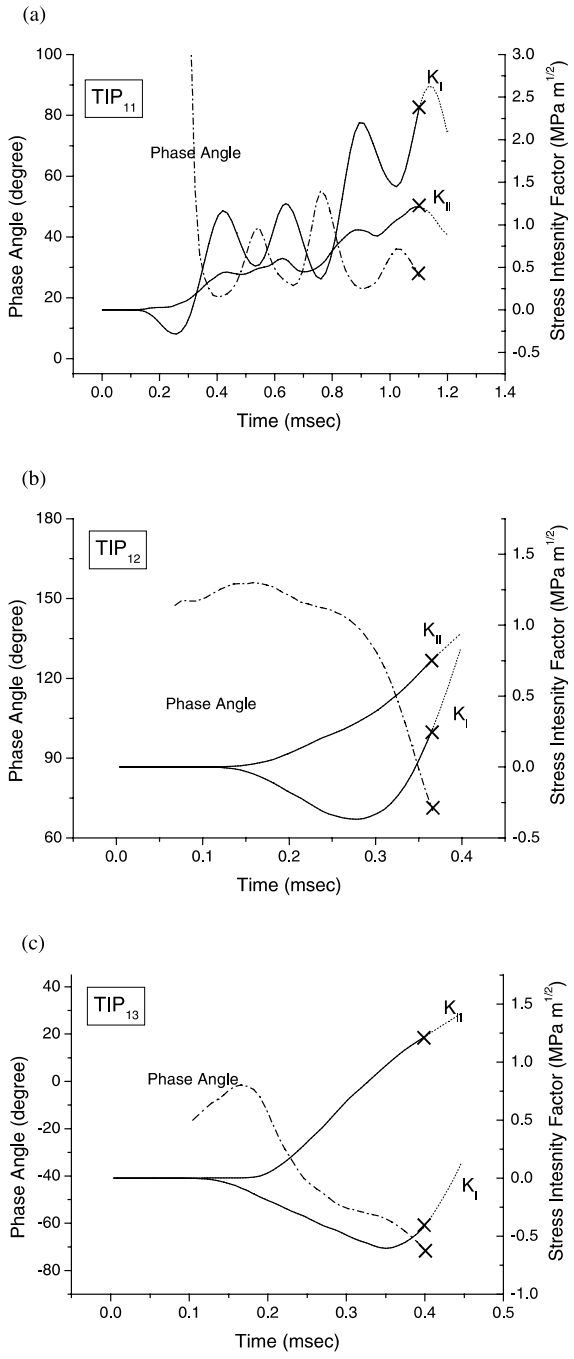

Fig. 8. Stress intensity factors and phase angle variation curve over time (× represents the onset of crack initiation).

contact of crack faces is not occurred yet. Deformed shape of TIP_{21} at the fractured time shows fully opened mode, but TIP_{23} shows closed mode behind the crack tip.

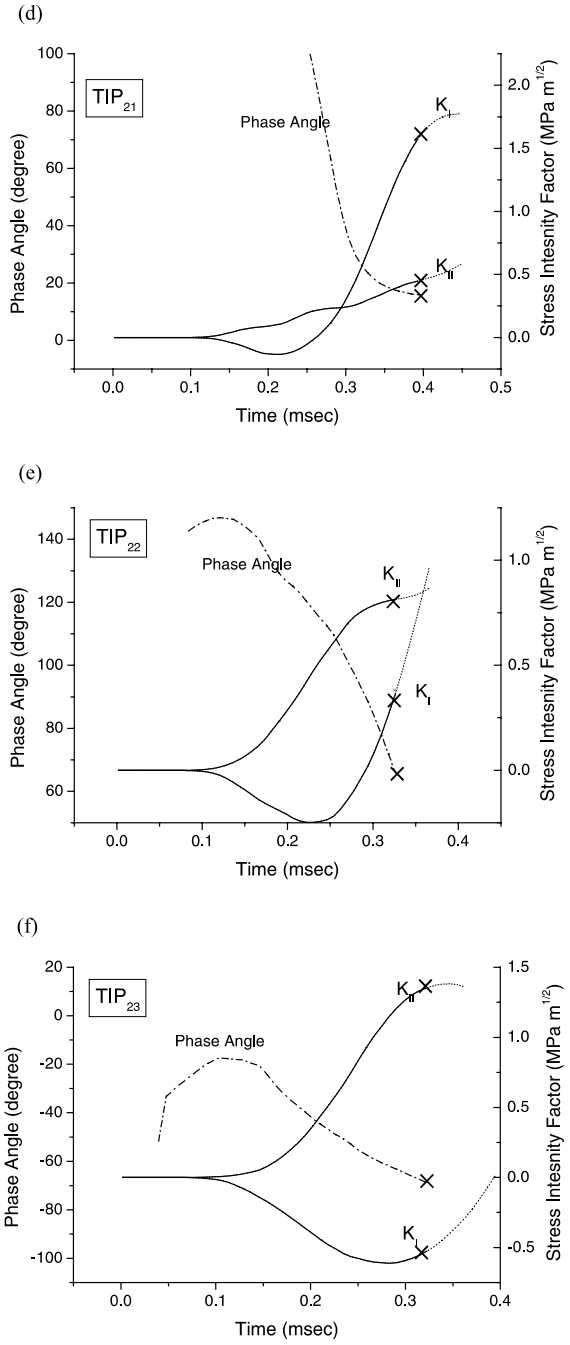

Fig. 8 (*continued*)

Another fracture parameter COD is observed at a distance 1000 μm behind the crack tip. COD is defined by a relative displacement of two. Fig. 10 shows COD for TIP_{22}. Solid line is calculated by Eq. (13) and dotted lines are calculated directly from FEM analysis. Two results calculated by Eq. (13) and crack model

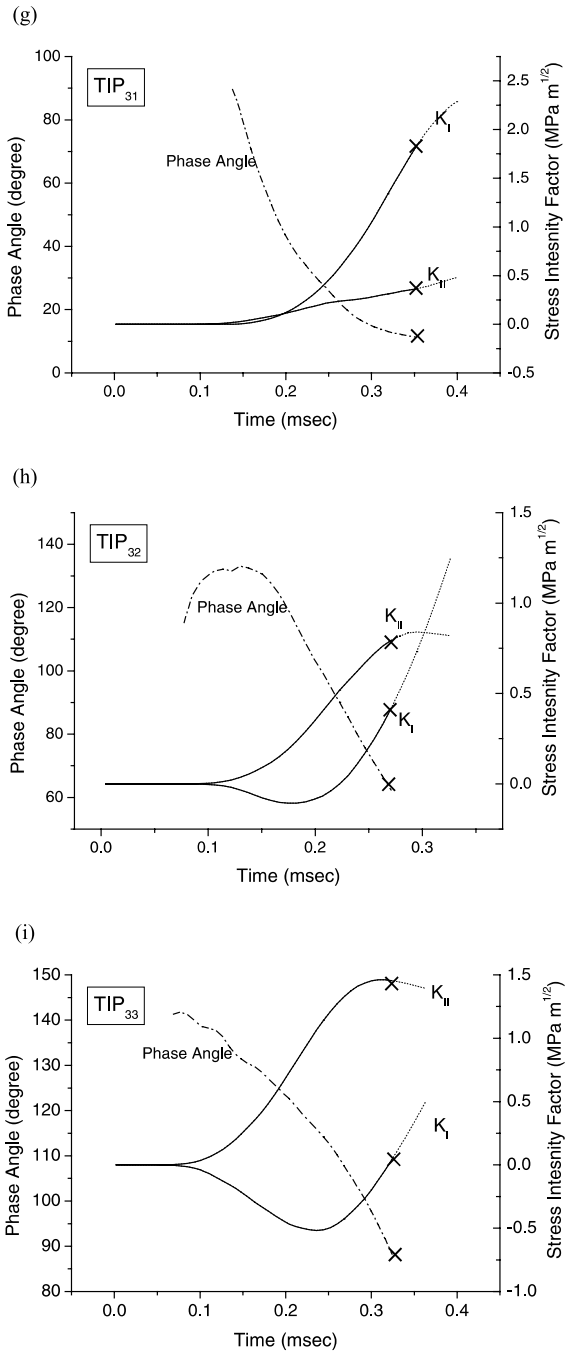

Fig. 8 (*continued*)

are nearly same. The result from wedge model shows a little difference, however, the difference is not much. Same results are obtained from the other TIPs. Therefore, COD can be used as fracture parameter of crack initiation. In the experiment, sometimes extraction of displacement is more convenient than stress intensity

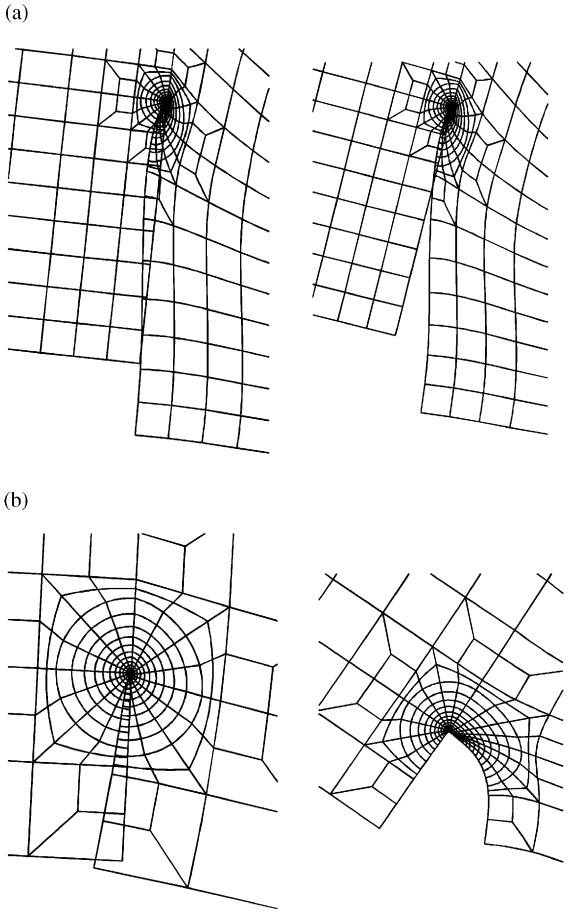

Fig. 9. Deformed shape of FEM model (magnification factor: ×200) (a) TIP_{23} at 0.28 and 0.32 ms (fractured); (b) TIP_{31} at 0.22 and 0.39 ms (fractured).

factors. Kavaturu and Shukla (1998) proposed the vectorial COD as fracture parameter of dynamically propagating interfacial crack.

The relationship between energy release rate, J, and phase angle, ψ, at the crack initiation time is shown in Fig. 11. Phase angle varies from 0° to 110°, and J varies from 100 to 550 Pam. TIPs 21 and 31 are collected around 10°. TIPs 12, 22, and 32 are collected around 65°. Finally, TIPs 13, 23, and 33 are collected around 100°. However, this figure shows roughly an unsymmetrical U shaped curve which had maximum at the TIP_{12} and TIP_{22} and had minimum values about 70° except for the TIP_{11}. One important point is TIP_{11}, that is, only one of five TIP_{11} specimens was fractured in this experiment. This behavior of TIP_{11} can be explained by the behavior of Figs. 7(a) and 8(a), that is, specimen of TIP_{11} shows much different variation behavior of J and K compared with the other TIPs. It seems that the current FEM model is insufficient in simulations for the case of TIP_{11}. The dependency of mode mixity on the energy release rate is also found in this Fig. 11, under the dynamic loading condition. This result of Fig. 11 shows good agreement with the static results of Liechti and Chai (1992) and the dynamic results of Tippur and Xu (1997).

To compare the dynamic result with the static result, a phase angle of the crack under the static condition at $J = 100$ Pam is shown in Fig. 12. All conditions of the FEM model are the same as dynamic conditions except that the external load is applied quasi-statically. All phase angles show plus values and

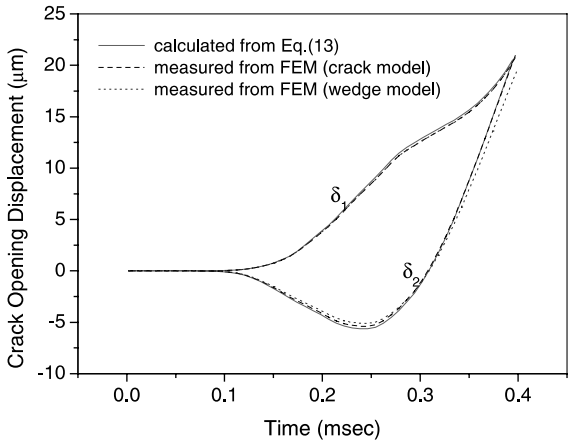

Fig. 10. COD for TIP_{22} at a distance 1000 μm behind the crack tip.

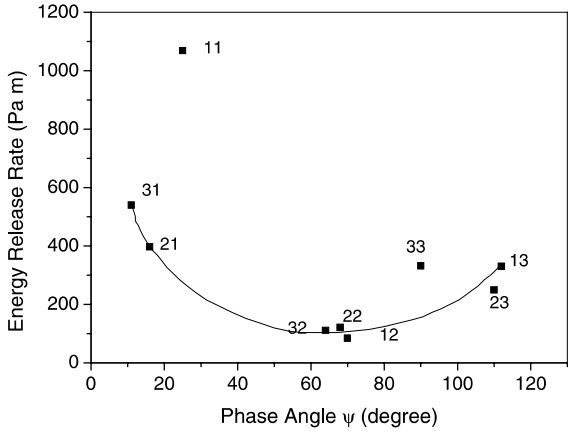

Fig. 11. Energy release rate and phase angle at the time when the crack initiates.

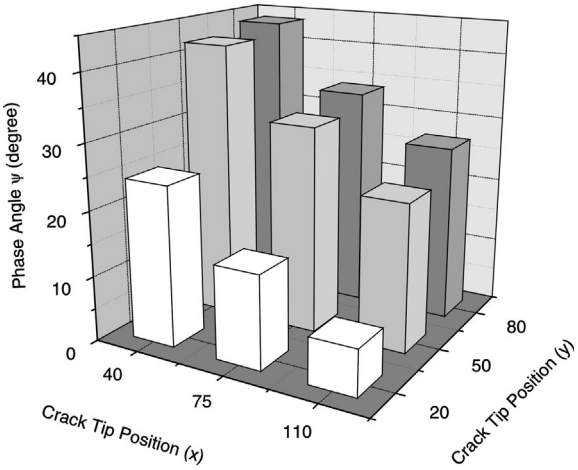

Fig. 12. Phase angle of stress intensity factors at each crack tip under the static condition.

vary from 10° to 45°. TIP_{31} shows minimum value. Therefore, it can be said that the estimation of the phase angle of the dynamic condition from the static result is not correct.

The magnitude of T stress has an effect on the shape and magnitude of the area of plastic deformation along with the stability of crack propagation (Larsson and Carlson, 1973). Fig. 13 shows T stresses of the

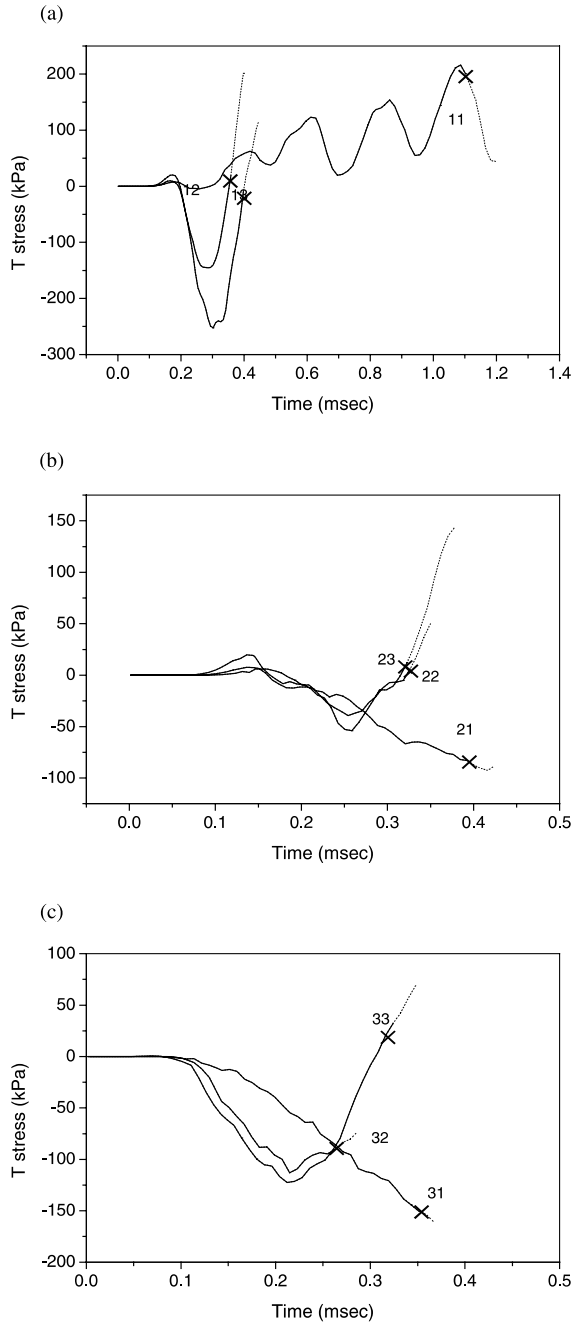

Fig. 13. T stress variation curve over time; (a) TIP_{1j}, (b) TIP_{2j}, (c) TIP_{3j} ($\times$ represents the onset of crack initiation).

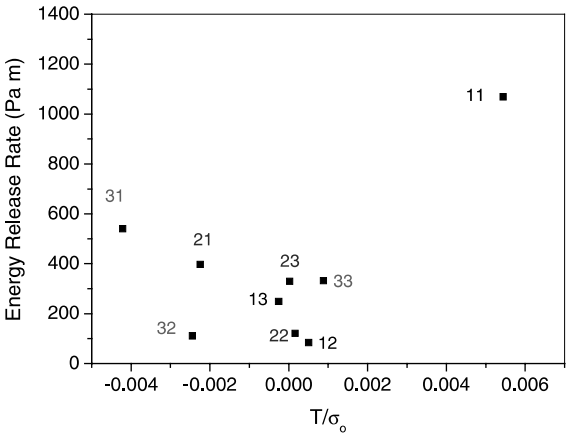

Fig. 14. Energy release rate and normalized T stress at the time when the crack initiates.

Table 2
The sign of T stress when crack initiates

$J=3$	≈ 0	≈ 0	≈ 0
$J=2$	≈ 0	≈ 0	$-$
$J=1$	$+$	$-$	$-$
	$I=1$	$I=2$	$I=3$

PMMA part. A variation curve of the T stress over time shows complex behavior, that is, T increases with (+) value at the first stage, and then decreases to (−) value and increases to (+) value again.

Fig. 14 shows the J–T relationship at the time when crack initiates. T stresses are normalized by yield stress σ_0 such as T/σ_0 (Rice, 1974). Yield stress σ_0(36.8 MPa) was measured by the use of tension specimen at room temperature according to ASTM 638 and 0.2% offset was applied. In this case, minimum T stress is -0.151 MPa on TIP_{31}, resulting in $T/\sigma_0 = -0.0041$. According to the result of Rice (1974), the shape of the plastic deformation area could be affected by T stress when T/σ_0 had order of 0.2. However, in this experiment, T stress is very small and the biaxiality parameter also shows small value $B = -0.019$. Therefore it seems that this magnitude of T stress has an insignificant effect on the behavior of a crack. Almost all values are distributed around zero except for the TIP_{11}. The sign of T stress, which is an important parameter of stability, is summarized in Table 2. At three TIPs (21, 31 and 32), T stresses are lower than zero. This indicates that the crack tends to propagate along the interface. In this experiment, actually it was observed that the length of interfacial crack at TIP_{31} was longer than that of TIP_{13} as shown in Fig. 6(a) and (b). Fig. 15 shows a biaxility parameter; (a) under the static condition and (b) under the dynamic condition. Under the static condition, biaxility parameter shows a small value from -0.02 to 0.08 which has a maximum at TIP_{13} and a minimum at TIP_{31}. Under the dynamic condition in Fig. 15(b), the change of magnitude is not significant when compared with the static condition, and a specific trend is not observed.

6. Conclusion

In this study, we studied low velocity impact responses of the fracture parameters of interfacial crack tips, such as energy release rate (J integral), stress intensity factors (K), COD, and T stress under a dynamic

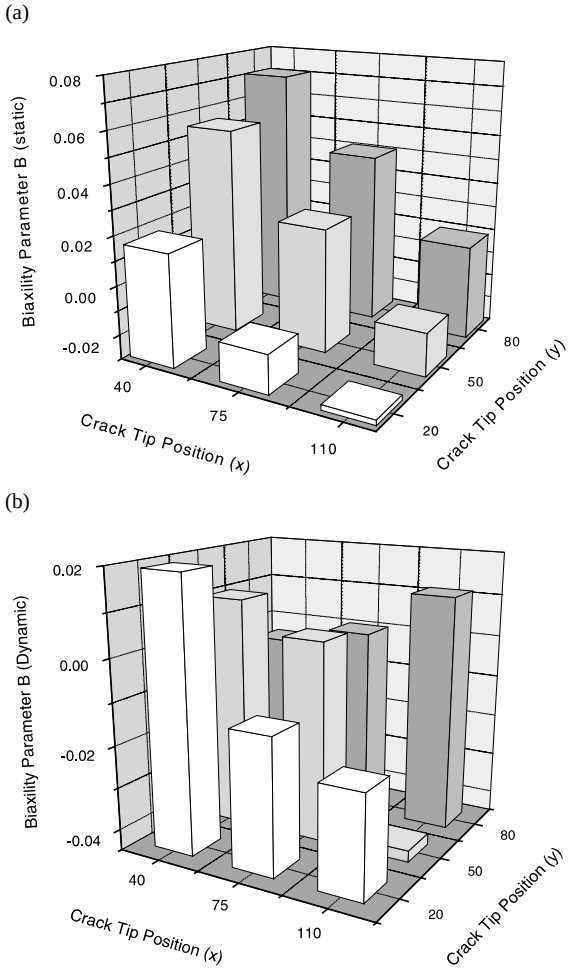

Fig. 15. Biaxility parameter at each crack tip; (a) under the static condition and (b) under the dynamic condition.

loading condition. A three point bending impact test was performed with bimaterial specimens composed of aluminum and PMMA. The crack initiation time was then measured by the grid line technique. Fracture parameters were calculated by the FEM and a programmed post processor.

As a result of this study we found the following results. Load signals of all specimens reached a peak in about 0.2 ms with the same inclination and roughly the same magnitude, and then diminished to zero after showing one or two more peaks. The interaction energy method showed good performance in the decomposition of the stress intensity factors and the calculation of elastodynamic T stress with path independency. The effects of J were not shown until about 0.2 ms, and then increased over time until it reach J_{ID}. Stress intensity factor and phase angle were calculated at a characteristic length 1000 μm. The phase angle of stress intensity factors varied with time. K_{II} increased with time, but K_I showed minus values at first and then increased to plus value. Therefore, crack closing effect was occurred at about 0.2–0.4 ms. Under the static condition, phase angle showed 10–45°, however, it expanded to 0–100° under the dynamic condition. Therefore the estimation of the phase angle of the dynamic condition from the static result was improper. The relationship between energy release rate, J, and phase angle, ψ, at the onset of crack

initiation showed unsymmetrical U shaped curve which had maximum at the TIP_{12} and TIP_{22} and had minimum values about 70°, except for the TIP_{11}. Through this result, mode mixity dependency on the energy release rate was found under the dynamic loading condition, similarly with the static condition. CODs calculated by FEM analysis and calculated by the equation of Rice were almost same. It was found that the magnitude of T stress was not enough to affect the plastic deformation. However, specimen whose T stress was less than zero showed stable crack growth along the interface, as expected in the analysis.

References

Atluri, S.N., 1986. Energetic approaches and path-independent integrals in fracture mechanics. Computational Methods in the Mechanics of Fracture. Elsevier, Amsterdam.

Cardew, G.E., Goldthorpe, M.R., Howard, I.C., Kfouri, A.P., 1985. On the elastic T-term. Fundamentals of Deformation and Fracture, Eshelby Memorial Symposium. Cambridge University Press, Sheffield.

Freund, L.B., 1990. Dynamic fracture mechanics. Cambridge University Press, Cambridge.

Johnson, K.L., 1987. Contact Mechanics. Cambridge University Press, Cambridge.

Kavaturu, M., Shukla, A., 1998. Dynamic fracture criteria for crack growth along bimaterial interfaces. J. Appl. Mech. 65, 293–299.

Kishimoto, K., Aoki, S., Sakata, M., 1980. On the path independent integral-J. Engng. Fract. Mech. 13, 841–850.

Lambros, J., Rosakis, A.J., 1995. Development of a dynamic decohesion criterion for subsonic fracture of the interface between two dissimilar materials. Proceedings of the Royal Society A 451, pp. 711–736.

Larsson, S.G., Carlsson, A.J., 1973. Influence of non-singular stress terms and specimen geometry on small-scale yielding at crack tips in elastic–plastic materials. J. Mech. Phys. Solids 21, 263–277.

Leevers, P.S., Radon, J.C., 1982. Inherent stress biaxility in various fracture specimen geometries. Int. J. Fract. 19, 311–325.

Li, F.Z., Shih, C.F., Needleman, A., 1985. A comparison of methods for calculating energy release rates. Engng. Fract. Mech. 21, 405–421.

Liechti, K.M., Chai, S.Y., 1992. Asymmetric shielding in interfacial fracture under in-plane shear. J. Appl. Mech. 59, 295–304.

Lo, C.Y., Nakamura, T., Kushner A, 1994. Computational analysis of dynamic crack propagation along a bimaterial interface. Int. J. Solids Struct. 31, 145–168.

Moon, H.J., Earmme, Y.Y., 1998. Calculation of elastic T-stresses near interface crack tip under in-plane and anti-plane loading. Int. J. Fract. 91, 179–195.

Rice, J.R., 1974. Limitations to the small scale yielding approximation for crack tip plasticity. J. Mech. Phys. Solids 22, 17–26.

Rice, J.R., 1988. Elastic fracture mechanics concepts for interfacial cracks. J. Appl. Mech. 55, 98–103.

Shih, C.F., Moran, B., Nakamura, T., 1986. Energy release rate along a three-dimensional crack front in a thermally stressed body. Int. J. Fract. 30, 79–102.

Sladek, J., Sladek, V., Pedelinski, P., 1997. Integral formulation for elastodynamic T-stresses. Int. J. Fract. 84, 103–116.

Suo, Z., 1989. Mechanics of Interface Fracture. Harvard University Press, Cambridge.

Tippur, H.V., Rosakis, A.J., 1991. Aqasi-static and dynamic crack growth along bimaterial interfaces: a note on crack-tip field measurements using coherent gradient sinsing. Exp. Mech. 31, 243–251.

Tippur, H.V., Xu, L., 1997. Interfacial crack initiation under quasi-static and dynamic loading conditions: an experimental study. Fatigue Fract. Engng. Mater. Struct. 20, 49–60.

Williams, M.L., 1957. On the stress distribution at the base of a stationary crack. J. Appl. Mech. 24, 109–113.